Solvothermal synthesis MgAl-LDH nanosheets

Katarina Cermelj[a], Kanittika Ruengkajorn[a], Jean-Charles Buffet[a], Dermot O'Hare[a]*

[a]Chemistry Research Laboratory, Department of Chemistry, University of Oxford, 12 Mansfield Road, Oxford, OX1 3TA, UK.
* Corresponding author: dermot.ohare@chem.ox.ac.uk

Abstract

A new solvothermal post-synthesis treatment for preparing high aspect ratio magnesium aluminium layered double hydroxides (MgAl-LDHs) has been developed. Treating laurate-intercalated MgAl-LDHs in pure ethanol in an autoclave for 48 hours at 150 ºC was found to produce delaminated MgAl-LDH nanosheets with a thickness of ~2.6 nm and an aspect ratio of ~105. It is proposed that the high pressure solvothermal process promotes the insertion of ethanol molecules into the LDH interlayer space, thereby facilitating delamination. This new post-synthesis treatment provides the opportunity for a facile, large scale route to highly delaminated high aspect ratio LDHs, which might be of interest towards novel nanomaterials for energy conversion and storage.

Keywords
Layered double hydroxide, Hydrophobicity, Aspect ratio, Solvothermal treatment, Delamination

1. Introduction

Layered double hydroxides (LDHs) are a family of host-guest type anionic clays with the general formula $[M^{z+}_{1-x}M'^{3+}_{x}(OH)_2]^{a+}$ $(X^{n-}_{a/n})\cdot bH_2O$, where usually $z = 2$, M^{2+} and M'^{3+} can be most divalent and trivalent cations, respectively, and X^{n-} can be a variety of anions. In the case of MgAl-LDHs, single phases exist only for $0.2 \leq x \leq 0.33$ [1-3]. The structure of an LDH is related to that of brucite, $Mg(OH)_2$, which consists of neutral layers of edge-sharing magnesium hydroxide octahedra [4]. In an LDH, partial isomorphous substitution of M^{2+} cations by M'^{3+} cations in the octahedral sites results in a net positive charge of the hydroxide layers, which is balanced by anions in the interlayer space [5].

Due to their compositional flexibility, high anionic exchange ability and biocompatibility, LDHs have a wide range of applications, acting as adsorbents in environmental purification [6-8], flame retardant materials [9-12], corrosion inhibitors [9,13], ion-exchange materials [1,9], polymer additives [10], and drug carrier agents [10,14]. Notably, LDHs have attracted significant attention as catalysts in a variety of energy conversion applications such as electrochemistry [7,15] and photocatalysis [16,17], as well as in energy storage applications [18]. For many of these applications, the morphology, and more specifically the aspect ratio of the LDH platelets (defined as platelet diameter/thickness) is a very important parameter to consider. For instance, Zhao *et al.* [19] have found that the particle diameter of NiTi-LDH

platelets plays an important role in determining their photocatalytic activity in the oxygen evolution reaction, whereas Dou *et al.* [20] have shown that the aspect ratio determines the gas barrier properties of LDH-containing polymer coatings. In general, the morphology and aspect ratio of LDHs can be controlled by careful adjustment of the synthetic conditions [20], and by carrying out suitable post-synthesis treatments [21-23].

The commonly used LDH synthesis methods include co-precipitation [6,9] and homogeneous precipitation [24] using an ammonia releasing reagent such as urea or hexamethylenetetramine (HMT) [25,26], with ageing at room temperature, and under refluxing [27,28] or hydrothermal conditions [26,29]. The specific choice of the synthesis method controls several important LDH properties, such as their chemical composition, morphology and degree of aggregation. Further fine-tuning of LDH properties is possible with the choice of post-synthesis treatment. The sample crystallinity may be improved through hydrothermal post-synthesis treatment, where Ostwald ripening also results in an increase in the LDH particle diameter and an improved particle morphology [3,23,30-33]. Other post-synthesis treatments have been developed with the aim of preparing LDH nanosheets. This has been achieved through delamination in a variety of polar solvents such as formamide, butanol and acrylates [34]. However, these methods do not enable the isolation of delaminated LDH nanosheets from such solvent dispersions without re-aggregation [22]. The synthesis of delaminated LDH dry powders presents a challenge that has been overcome in the aqueous miscible organic solvent treatment (AMOST) method developed by Wang *et al*. [22,35] who reported the first example of LDH powders that still remain exfoliated on drying.

An alternative delamination method has been developed for the preparation of graphene from graphite, where a solvothermal-assisted exfoliation is carried out in a highly polar organic solvent, acetonitrile, under solvothermal conditions in a Teflon-lined autoclave at 180 ºC for 12 hours [36]. It has been proposed that the high pressure established within the autoclave promotes the insertion of acetonitrile molecules into the interlayer region of expanded graphite, thereby facilitating its delamination.

In addition to the aspect ratio, the hydrophobicity or hydrophilicity of the LDH material also determines its suitability for different applications. Inorganic LDHs, such as carbonate-containing CO_3-LDHs, are hydrophilic because of the surface hydroxyl groups and the layer of inorganic anions on the outer LDH surface, all of which can form hydrogen bonds to water molecules in the solvation shells of LDH particles [37,38]. On the other hand, organophilic LDHs (organo-LDHs) with intercalated organic anions are hydrophobic, which allows them to be better dispersed in a variety of non-polar solvents and therefore extends the range of possible LDH applications. Furthermore, while high aspect ratio hydrophilic LDHs have been extensively studied [20,39], little research has been done in the area of hydrophobic high aspect ratio LDHs.

Herein, the effect of the reaction conditions on the properties of laurate-intercalated MgAl-LDHs (MgAl-LR-LDHs) has been systematically investigated in order to develop an optimised procedure for the preparation of pure, single phase, crystalline MgAl-LR-LDHs. Following the optimisation of the reaction conditions, the AMOST post-synthesis treatment was carried out

on the optimised products, and found to result in only partial delamination. The solvothermal-assisted exfoliation typically applied to graphite in the production of graphene was adapted, and found to be highly successful in producing delaminated high aspect ratio MgAl-LR-LDH nanosheets.

2. Experimental

2.1 Preparation of MgAl-LR-LDHs

The Mg_3Al-LR-LDHs were synthesised via a co-precipitation and two different homogeneous precipitation methods. The co-precipitation method was adapted from Wang *et al.* [22,35]. $Mg(NO_3)_2{\cdot}6H_2O$ (9.62 g, 37.5 mmol) and $Al(NO_3)_3{\cdot}9H_2O$ (4.69 g, 12.5 mmol), Mg:Al molar ratio 3:1, were dissolved in 100 mL DI water (Solution A). Lauric acid (2.40 g, 12.0 mmol) was dissolved in 150 mL DI water at 80 °C and the pH was adjusted to 10 by dropwise addition of 4 M NaOH (Solution B). Solution A was added to Solution B dropwise over the period of 1 hour with vigorous stirring and the pH of the precipitation was maintained at ~10 using 4 M NaOH solution. The resulting reaction mixture was aged in an oil bath heated at 105 °C for 18 hours with stirring at 700 rpm. After ageing, the LDH products were washed with 1 L of 1:1 mixture of ethanol and DI water at 80 °C, followed by drying overnight in a vacuum oven at room temperature.

The homogeneous precipitation methods were adapted from Costantino *et al.* (urea method) [24] and Ogawa *et al*. (urea hydrothermal method) [40]. $Mg(NO_3)_2{\cdot}6H_2O$ (9.62 g, 37.5 mmol), $Al(NO_3)_3{\cdot}9H_2O$ (4.69 g, 12.5 mmol), Mg:Al molar ratio 3:1, and urea (15.01 g, 250.0 mmol) were dissolved in 200 mL DI water (Solution C). Lauric acid (2.40 g, 12.0 mmol) was dissolved in 50 mL DI water at 80 °C and the pH was adjusted to 10 by dropwise addition of 4 M NaOH (Solution D). Solution C was added to Solution D during vigorous stirring. For the urea reflux method, the resulting reaction mixture was aged in an oil bath heated at 105 °C for 18 hours with stirring at 700 rpm. For the urea hydrothermal method, 40 mL of the reaction mixture was transferred to a 50 mL Teflon inner vessel within a stainless steel outer vessel, followed by ageing in an oven pre-heated at 105 °C for 18 hours. After ageing, the LDH products were washed with 1 L of 1:1 mixture of ethanol and DI water at 80 °C, followed by drying overnight in a vacuum oven at room temperature.

2.2 Post-synthesis treatments of MgAl-LR-LDHs

The wet cake Mg_3Al-LR-LDH prepared by the urea reflux method was treated using the AMOST washing procedure, which was adapted from literature [22,35,41]. After ageing, the LDH was washed with 1 L of 1:1 mixture of ethanol and DI water at 80 °C and the wet cake was dispersed in 250 mL of aqueous miscible organic (AMO) solvent until a well dispersed slurry was obtained. The slurry was filtered and re-dispersed in 500 mL of AMO solvent and left to stir at 800 rpm for 4 hours. Finally, the resulting AMO-LDH was filtered, washed with 250 mL of AMO solvent and dried overnight in a vacuum oven at room temperature. Two different AMO solvent were used, ethanol and acetone.

The dry powder Mg_3Al-LR-LDH prepared by the urea reflux method was treated using the solvothermal post-synthesis treatment. Dry powder (2.50 g) was dispersed in 25 mL of ethanol, and the dispersion transferred into a 50 mL Teflon inner vessel within a stainless steel outer vessel. The solvothermal treatment was carried out at 150 °C for 4, 6, 8, 24 or 48 hours. Following the solvothermal treatment, the autoclaves were placed into cold water to cool and each organo-LDH product was washed with 200 mL of ethanol, followed by drying overnight in a vacuum oven at room temperature.

2.3 Structure, composition and morphology characterisation

The product purity, crystallinity and structure were analysed by powder X-ray diffraction (PXRD, PANalytical X'pert Pro) using Cu K_α radiation within the 2θ range 2º – 70º. The presence and nature of intercalated anions was confirmed by Fourier transform infrared (FTIR) spectroscopy, in the range 700 – 4,000 cm^{-1} with 50 scans at 4 cm^{-1} resolution. The hydrophobicity of the samples was investigated by measuring the contact angles of water droplets deposited on top of the LDH powder, which was adhered to a glass microscope slide using double sided tape. The elemental composition of samples was analysed by the quantitative combustion technique. The composition of the samples was further characterised by thermogravimetric analysis (TGA) under a continuous flow of N_2 from 30 to 600 °C at a rate of 10 °C/minute. The morphology of the samples was investigated using transmission electron microscopy (TEM, Jeol JEM-2100 at 200kV). ^{27}Al DP MAS and ^{13}C CP MAS solid state NMR spectra were collected at 104.2 and 100.5 MHz, respectively, on a Bruker Avance III HD 400 spectrometer. The ^{27}Al NMR chemical shift is referenced to an aqueous solution of $Al(NO_3)_3$ (0 ppm) and the ^{13}C spectra were referenced to adamantane (the upfield resonance was taken to be δ = 29.5 ppm on a scale where δ(TMS) = 0) as a secondary reference [42].

3. Results and discussion

3.1 Variation of MgAl-LR-LDH synthesis method

To determine the optimum synthesis method for the preparation of pure, crystalline Mg_3Al-LR-LDHs, co-precipitation, urea reflux and urea hydrothermal synthesis methods were investigated. The basal spacing, as determined by PXRD, of Mg_3Al-LR-LDHs prepared by all three synthesis methods is ~24.5 Å (Figure 1), which is in good agreement with the previously reported laurate monolayer formation in the LDH interlayer space [26,27,43]. The three products have different degrees of crystallinity, with the co-precipitation product being least crystalline, as evidenced by reduced peak intensities and broadened PXRD reflections. Both homogeneous precipitation products are more crystalline, but the urea hydrothermal product contains two impurity phases: hydromagnesite, $Mg_5(CO_3)_4(OH)_2{\cdot}4H_2O$, and $MgAl$-CO_3-LDH, the latter exhibiting a typical basal spacing of ~7.6 Å [24]. Both arise because the CO_2 gas generated during the urea hydrolysis cannot leave the closed autoclave system, thus generating a significant amount of CO_3^{2-} in the reaction mixture.

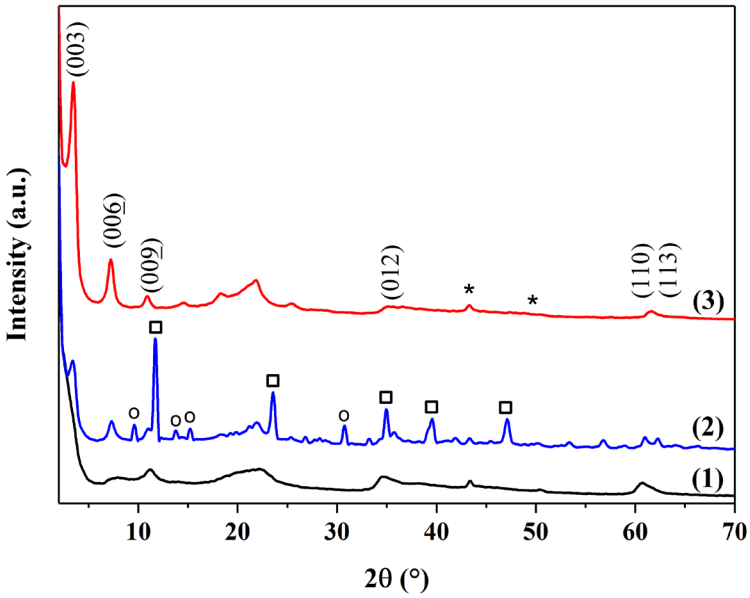

Figure 1 PXRD patterns of Mg_3Al-LR-LDHs prepared by (1) co-precipitation, (2) urea hydrothermal and (3) urea reflux methods. ○ denotes characteristic hydromagnesite peaks, □ denotes MgAl-CO_3-LDH peaks and * denotes sample holder peaks.

The urea reflux method product comprises a pure Mg_3Al-LR-LDH phase with high crystallinity. Its PXRD pattern is typical of a carboxylate intercalated LDH with three major (00*l*) basal reflections in the 0 – 15° 2θ region, corresponding to the (003), (006) and (009) Bragg reflections [44]. The broad, poorly resolved feature at ~20° (d ~4.3 Å) can be attributed to the lateral stacking of the organic anion alkyl chains in the LDH interlayer space [26,45].

The FTIR spectra of Mg_3Al-LR-LDHs synthesised by the three different methods are compared in Figure 2. All three spectra show bands characteristic of an LDH with intercalated carboxylate anions. The presence of laurate anions is demonstrated by the bands due to the asymmetric and symmetric C-O and C-H stretching vibrations [26,27,45,46]. The band due to the asymmetric stretching mode of CO_3^{2-} (ν_3 in D_{3h} symmetry) at ~1,360 cm^{-1} is only present in products of the urea hydrothermal and co-precipitation methods, thus confirming that the urea method product is free of carbonate containing impurities [27,46].

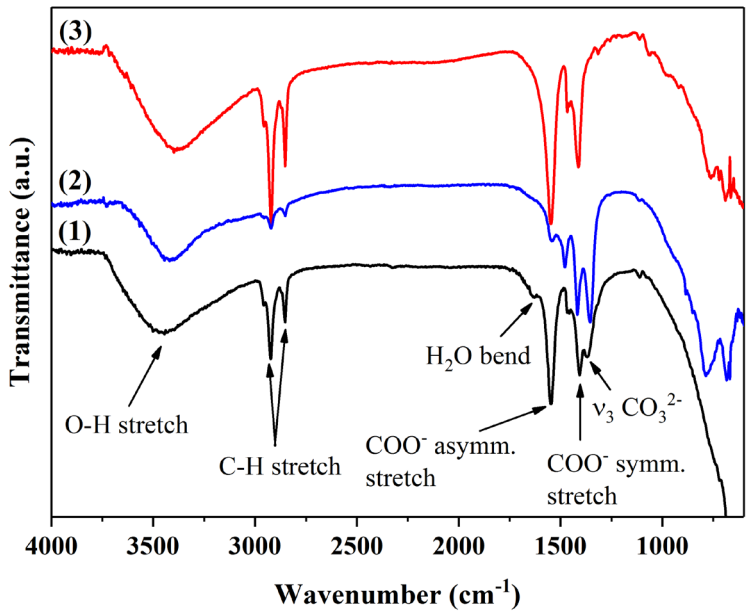

Figure 2 FTIR spectra of Mg_3Al-LR-LDHs prepared by (1) co-precipitation, (2) urea hydrothermal and (3) urea reflux methods.

The structure and morphology of Mg_3Al-LR-LDHs synthesised by the three different methods were investigated by TEM (Figure 3-a,b,c). Both the co-precipitation and the urea reflux products consist of thin sheet-like particles with curved and irregular contours. The urea hydrothermal method product has a noticeably different morphology, with platelets roughly hexagonal in shape that appear individually, in small stacks, and in flower-like aggregates. The significant change in particle morphology between the urea and urea hydrothermal methods highlights the importance of pressure in increasing the LDH product crystallinity and particle size, which has been noted previously [23].

The urea reflux method was chosen for further analysis and post-synthesis treatments, as it produces pure Mg_3Al-LR-LDH products with good crystallinity. It is thus superior to the co-precipitation method, which generates poorly crystalline products, as well as to the urea hydrothermal method, which despite producing the best particle morphology, results in organo-LDH products containing MgAl-CO_3-LDH and hydromagnesite impurities.

The hydrophobicity of the urea reflux product was investigated by measuring the contact angles of water droplets deposited on top of the LDH powder. The observed contact angle is 152º (Figure 3-d), which therefore indicates that the MgAl-LR-LDH product prepared by the urea reflux method is a superhydrophobic material [47,48].

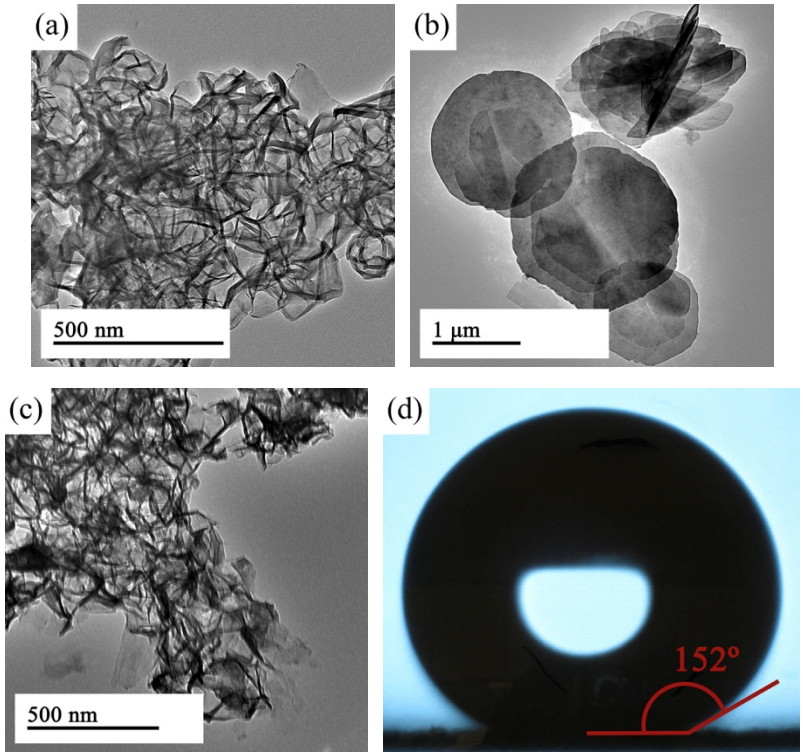

Figure 3 TEM images of Mg_3Al-LR-LDHs prepared by (a) co-precipitation, (b) urea hydrothermal and (c) urea reflux methods. (d) The shape of a water droplet deposited on top of the MgAl-LR-LDH powder, prepared by the urea reflux method.

In order to elucidate the molecular formula of the Mg_3Al-LR-LDH synthesised by the urea reflux method, TGA and elemental analysis were used. Theoretical predictions of the C and H contents were based on the initially assumed molecular formula of $[Mg_3Al(OH)_8](C_{12}H_{23}O_2)\cdot 2H_2O$ [21]. The larger than expected C content determined by elemental analysis implies the presence of excess lauric acid that has not been removed during the washing process (Table S1).

The TGA and dTGA curves for the urea reflux method product (Figure S1) are characteristic of an organo-LDH with the weight loss up to ~220 °C corresponding to the loss of interlayer and adsorbed water, and the broad dTGA peak at ~400 °C corresponding to combined metal hydroxide layers dehydroxylation and laurate anion decomposition [49]. The first weight loss in the TGA plot gives a value of ~3.7 for the number of water molecules per formula unit. Therefore, the corrected molecular formula of the product obtained by a urea reflux is $[Mg_3Al(OH)_8](C_{12}H_{23}O_2)\cdot 3.7H_2O\cdot 0.3(C_{12}H_{24}O_2)$, which is in good agreement with elemental analysis.

3.2 AMO solvent post-synthesis treatment of MgAl-LR-LDH

The AMO solvent post-synthesis treatment was carried out on the product of the urea reflux method, using either ethanol or acetone as the AMO solvent in the re-dispersion of the washed wet cake organo-LDH [21,22]. The PXRD patterns of the AMO-Mg_3Al-LR-LDHs show little difference from the starting materials (Figure 4).

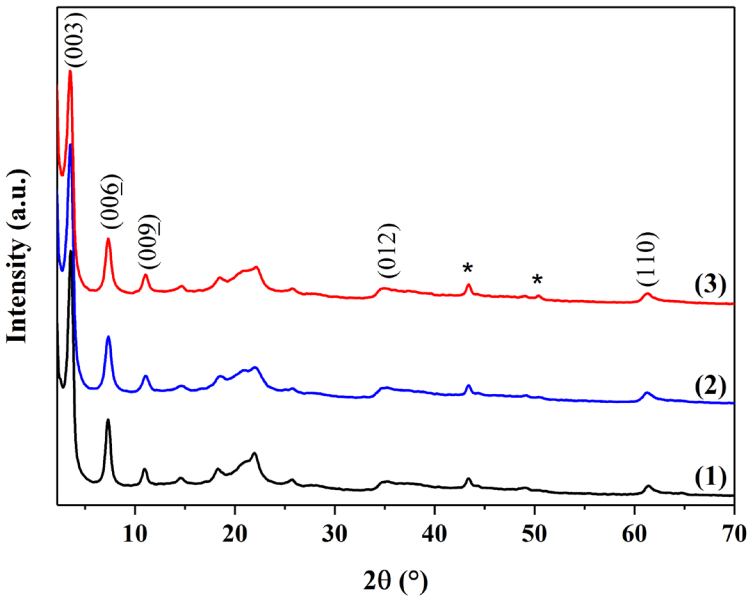

Figure 4 PXRD patterns of AMO-Mg_3Al-LR-LDHs: (1) water washed starting material, (2) acetone washed, and (3) ethanol washed. * denotes sample holder peaks.

There is a slight peak broadening and reduction in peak intensity of the (00*l*) peaks, indicating that a negligible degree of delamination takes place [22,50]. This contrasts with the complete delamination into single layer nanosheets of Zn_2Al- and Mg_3Al-borate-LDHs by the AMOST method reported previously [22,50]. The feature at ~20° changes after treatment with AMO solvent, indicating a change in packing arrangement of the laurate anions in the interlayer region [26,45].

Similarly, the FTIR spectra show no significant difference between the AMO-LDHs and the starting materials (Figure S2) which is consistent with the AMO solvent being present in the LDH in too small quantities to be detected by PXRD or FTIR spectroscopy [21].

In terms of morphology, the AMO-organo-LDH products are a mixture of two morphologies (Figure 5), one consisting of ~7 nm thin delaminated sheets, and the other resembling that of the water-washed non-AMO product but with reduced aggregation. It is the latter morphology that gives rise to the (00*l*) peaks in the PXRD patterns (Figure 4-2,3) since the delaminated sheets are so thin that there is insufficient coherence along the platelet stacking axis (*c*-axis) to observe any significant contribution to (00*l*) Bragg reflection intensity [22].

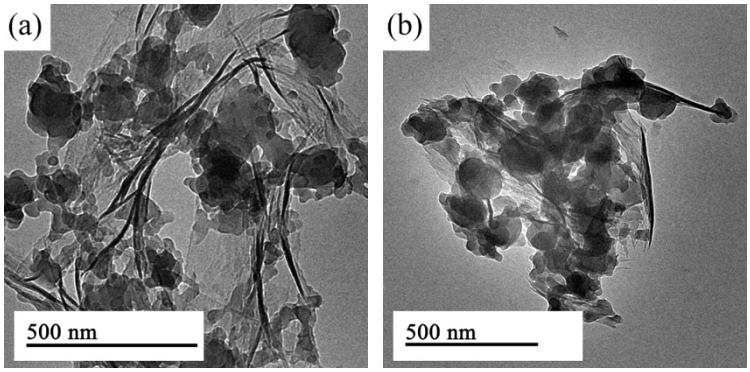

Figure 5 TEM images of AMO-Mg_3Al-LR-LDHs, with the AMO solvent being (a) acetone and (b) ethanol.

It is therefore evident that while AMO solvent post-synthesis treatment does reduce the aggregation of the organo-LDH products, it is not effective in generating high aspect ratio particles by means of delamination.

3.2 Solvothermal post-synthesis treatment of MgAl-LR-LDH

Solvothermal treatment was carried out on the dry powder Mg_3Al-LR-LDH, synthesised by the urea reflux method, in pure ethanol at 150 °C, with the treatment time being varied between 4, 6, 8, 24 and 48 hours.

The PXRD patterns of Mg_3Al-LR-LDH products after solvothermal treatment in Figure 6 show that the treatment effects are more pronounced for longer treatment times, with noticeable peak broadening and reduced peak intensity of the (00*l*) peaks as the treatment time is increased from 6 to 24 hours. Furthermore, the (00*l*) peaks in the PXRD patterns in Figure 6-2,3 shift to smaller angles, such that the basal spacing of the product after solvothermal treatment at 150 °C for 24 hours is ~26.4 Å. This may be the consequence of either an increased amount of ethanol solvent molecules in the LDH interlayer space, or of the hydroxide ions in the metal hydroxide layers being partially replaced by ethoxide ions formed from the treatment solvent. The peak profile at ~20° gets broader and less well-defined, which implies a greater number of possible stacking arrangements of the laurate anions. This greater disorder in their arrangement is consistent with a larger proportion of laurate being located at the LDH particle surface rather than in the more ordered interlayer regions as delamination produces thinner particles with fewer layers.

As can be seen in Figure 6-3, the 24 hour solvothermal treatment is insufficient to achieve full delamination. Therefore, the treatment time was extended to 48 hours, and the absence of distinct (00*l*) peaks in the corresponding PXRD pattern for the prolonged solvothermal treatment product (Figure 6-4) indicates that full delamination was achieved. Thus, the organo-LDH exists entirely in the form of nanosheets that are so thin that there is insufficient coherence along the platelet stacking axis (*c*-axis) to observe any (00*l*) Bragg reflection intensity [22].

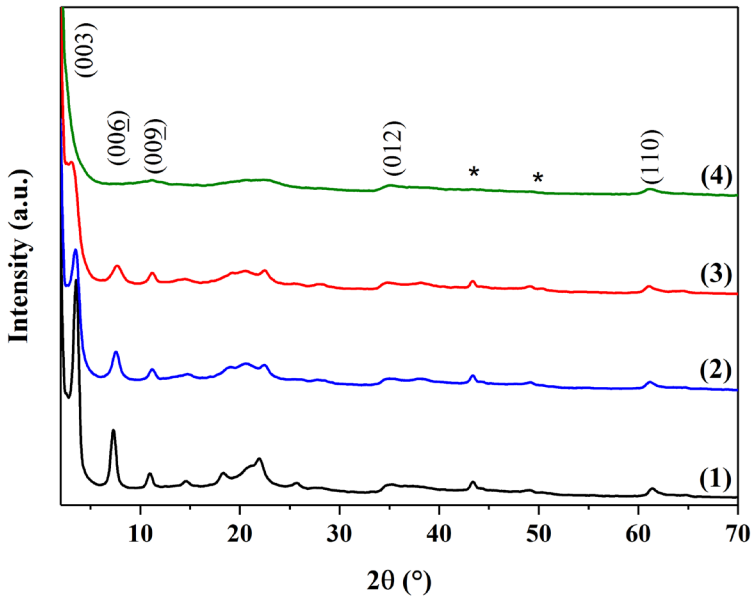

Figure 6 PXRD patterns of Mg_3Al-LR-LDHs after solvothermal treatment at 150 °C for (1) 0 hours, (2) 6 hours, (3) 24 hours, (4) 48 hours. * denotes sample holder peaks.

The FTIR spectra of Mg_3Al-LR-LDHs do not change significantly after the solvothermal treatment (Figure S3). Most notably, the presence of a band at ~1,050 cm^{-1} indicates the incorporation of ethanol (or ethoxide) into the organo-LDHs [51].

Similarly to AMO-organo-LDHs, the product after the 24 hour solvothermal treatment is a mixture of two morphologies (Figure 7-a): the irregularly shaped particles that are the remnant of the original urea reflux product, and the delaminated nanosheets comprising fewer metal hydroxide layers. Specifically, the sheets are ~2.6 nm thin, which is a noticeable difference from the ~7.0 nm in the AMO-organo-LDH case. The value of ~2.6 nm is an average taken over several LDH nanosheets, and in conjunction with the basal spacing of ~26.4 Å determined from PXRD (Figure 6-3), indicates that the delamination process generates a mixture of monolayer and bilayer LDH particles.

Prolonging the solvothermal treatment time to 48 hours results in the organo-LDH comprising solely ~2.6 nm thin nanosheets (Figure 7-b). This is consistent with the PXRD pattern in Figure 6-4 having no distinct (00*l*) peaks [22]. The average diameter of the sheets is ~272 nm, corresponding to an aspect ratio of ~105. Although higher MgAl-LDH aspect ratios have been reported [20,39], this is the highest aspect ratio of organo-LDHs obtained by direct synthesis to date [43,52,53].

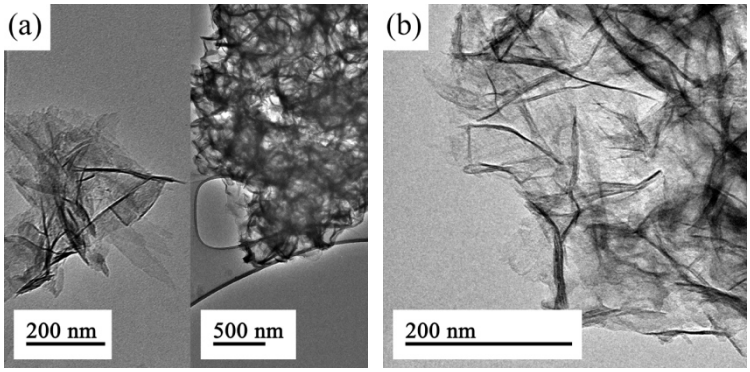

Figure 7 TEM images of Mg_3Al-LR-LDHs after solvothermal treatment at 150 °C for (a) 24 and (b) 48 hours.

The complexity of TGA and dTGA curves of the Mg_3Al-LR-LDHs increases after the 48 hour solvothermal post-synthesis treatment (Figure S4). The TGA curve observed is unlike those found in literature for carboxylate-intercalated LDHs [49]. To gain further insight, the product of the 48 hour treatment was investigated by elemental analysis (Table S2) as well as ^{13}C CP MAS and ^{27}Al DP MAS NMR spectroscopy (Figure 8).

The smaller than expected C content determined by elemental analysis is a consequence of part of the laurate anions being replaced by ethoxide ions during the solvothermal treatment, as it is carried out in pure ethanol. However, the dTGA peak at ~80 °C in Figure S4 indicates the presence of ethanol, which needs to be present in smaller quantities than ethoxide to result in a reduced C content. The weight loss at ~290 °C therefore corresponds to ethoxide decomposition. The reduced amount of laurate results in a smaller weight loss in the region above 300 °C as compared to the non-treated urea reflux product. The replacement of part of the laurate ions with ethoxide ions is also consistent with the reduced H content.

The ^{13}C CP MAS NMR spectra (Figure 8-a) confirm that the Mg_3Al-LR-LDH products both before and after the 48 hour solvothermal treatment contain laurate anions [44]. Furthermore, the ^{13}C CP MAS NMR spectrum of the solvothermal treatment product verifies the presence of ethanol or ethoxide. The ^{27}Al DP MAS NMR spectra (Figure 8-b) show the presence of two aluminium environments corresponding to octahedral aluminium at 8.01 and 9.22 ppm, and tetrahedral aluminium at 65.03 and 69.55 ppm, for the organo-LDH product before and after the solvothermal treatment, respectively [44,54]. Additionally, an extra resonance appears in the tetrahedral aluminium region around 81.20 ppm for the product after the treatment.

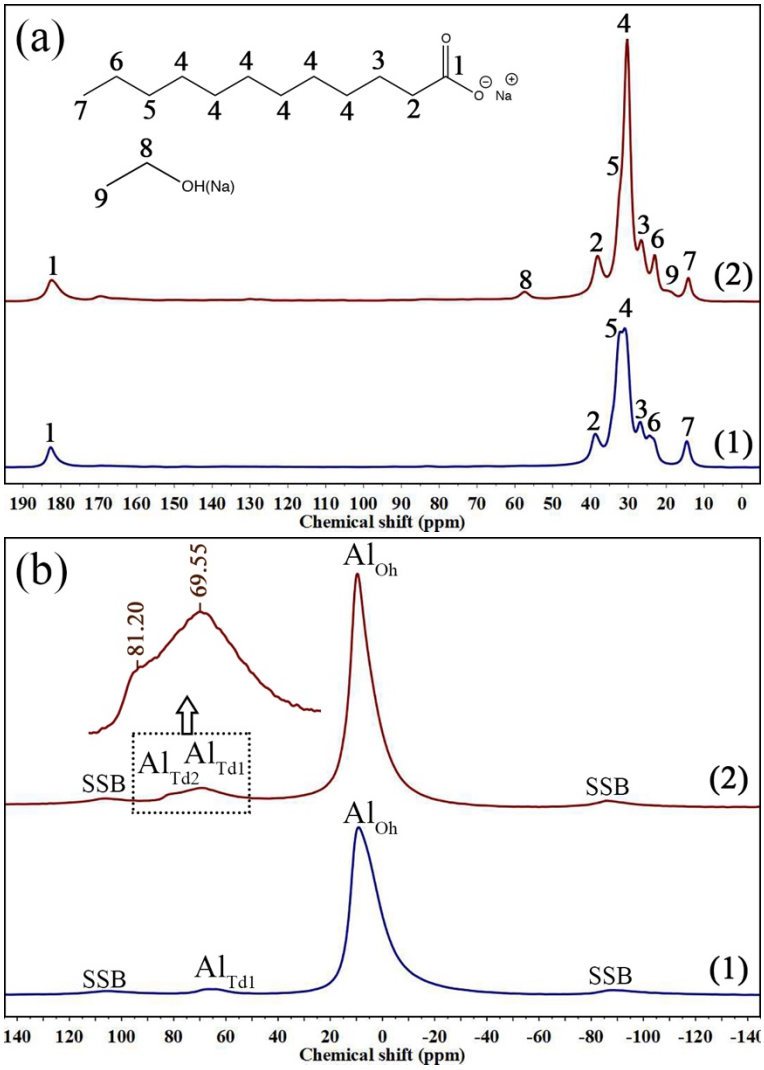

Figure 8 (a) ^{13}C CP MAS and (b) ^{27}Al DP MAS NMR spectra of Mg_3Al-LR-LDH (1) before and (2) after solvothermal treatment at 150 °C for 48 hours. The resonance at around 170 ppm in the ^{13}C spectrum of the solvothermal treatment product is due to carbonate anions [44]. SSB refers to spinning side bands.

The second tetrahedral aluminium environment may be due to part of the ethoxide ions displacing some of the hydroxide ions in the metal hydroxide layers [51], thereby changing the local environment around a proportion of the aluminium cations. This is consistent with the resonance of tetrahedral aluminium occurring at ~70 ppm in the case of both aluminium hydroxide and aluminium ethoxide [55,56]. This change in the composition of the metal hydroxide layers explains the shift of the dTGA peak corresponding to laurate decomposition and dehydroxylation to a higher temperature as compared to the non-treated organo-LDH (Figure S4). It is also consistent with the increase in the basal spacing seen in Figure 6-2,3. Therefore, the 48 hour solvothermal treatment product can be formulated as $[Mg_3Al(OH)_{8-x}(C_2H_5O)_x](C_{12}H_{23}O_2)_{1-y}(C_2H_5O)_y \cdot aH_2O \cdot b(C_2H_6O)$.

While further studies are required to fully elucidate the mechanism of the solvothermal treatment-induced delamination, it is likely that it proceeds in a manner similar to the solvothermal-assisted exfoliation of graphite to form graphene, which was developed by Qian *et al.* [36] in 2009. They suggested that the high pressure established within the autoclave allows the insertion of acetonitrile molecules into the graphite interlayer region. Similarly, the

high pressure established during the solvothermal treatment in this work promotes the migration of ethanol molecules into the MgAl-LR-LDH interlayer region, thereby facilitating delamination into ~2.6 nm thin nanosheets. The proposed mechanism is illustrated in Figure 9.

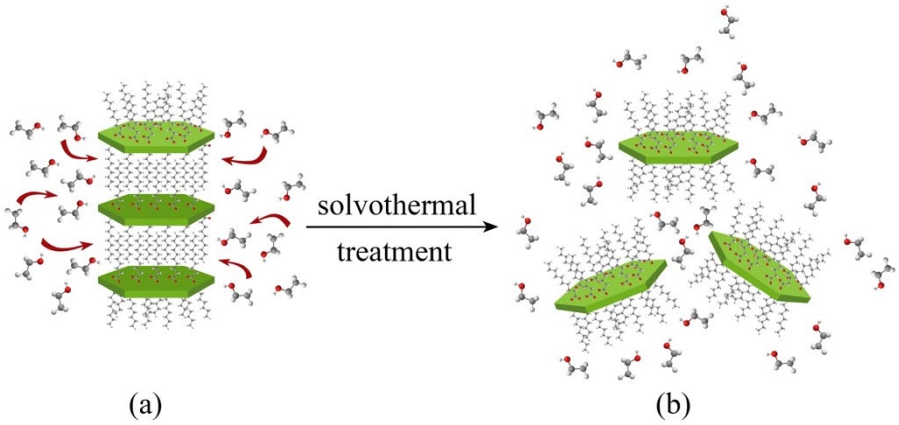

Figure 9 Schematic illustration of the solvothermal treatment-induced delamination of MgAl-LR-LDH: (a) insertion of ethanol molecules into the LDH interlayer region facilitated by the high pressure, and (b) the delaminated LDH nanosheets.

4. Conclusions

We report a simple and scalable route for the preparation of high aspect ratio delaminated MgAl-LR-LDH nanosheets using a solvothermal post-synthesis procedure. A systematic investigation of three different synthesis methods was carried out, and it was shown that the urea reflux method produces MgAl-LR-LDHs with the highest degree of purity and crystallinity. The AMOST post-synthesis treatment was found to decrease the amount of sample aggregation, but resulted in only partial LDH particle delamination. A new solvothermal post-synthesis treatment was developed, where the surfactant-intercalated MgAl-LR-LDHs were treated in pure ethanol in an autoclave at 150 ºC. The greatest degree of delamination was obtained for the longest treatment time of 48 hours, which produced MgAl-LR-LDH nanosheets with an average thickness of ~2.6 nm and a corresponding aspect ratio of ~105. Crucially, the organo-LDH powder remains delaminated on drying, as shown by PXRD analysis. We suggest that the solvothermal treatment-induced LDH delamination proceeds via the insertion of ethanol molecules into the LDH interlayer region, which is enabled by the high pressure established in the autoclave. The ability to increase the LDH particle aspect ratio provided by this new post-synthesis treatment should allow greater control over the activity of LDH materials in their photocatalytic and electrochemical applications. Further studies into the exact mechanism and the effects of this solvothermal post-synthesis treatment on the catalytic behaviour of LDHs with different intercalated species and metal cation compositions are on-going.

Acknowledgements

The authors would like to thank SCG Chemicals Co Ltd and SCG Packaging Co Ltd, Thailand, for funding, Dr Nick Rees (University of Oxford) for solid state NMR analysis, and KC acknowledges the AdFutura scholarship provided by the Slovene Human Resources Development and Scholarship Fund.

References

[1] A.I. Khan, D. O'Hare, J. Mater. Chem. 12 (2002) 3191–3198.
[2] G.W. Brindley, S. Kikkawa, Am. Mineral. 64 (1979) 836–843.
[3] S. Miyata, Clays Clay Miner. 28 (1980) 50–56.
[4] W. Reichle, Solid State Ionics 22 (1986) 135–141.
[5] L. Pesic, S. Salipurovic, V. Markovic, D. Vucelic, W. Kagunya, W. Jones, J. Mater. Chem. 2 (1992) 1069–1073.
[6] S.P. Newman, W. Jones, New J. Chem. 22 (1998) 105–115.
[7] C. Li, M. Wei, D.G. Evans, X. Duan, Small 10 (2014) 4469–4486.
[8] K.-H. Goh, T.-T. Lim, Z. Dong, Water Res. 42 (2008) 1343–1368.
[9] F. Cavani, F. Trifirò, A. Vaccari, Catal. Today 11 (1991) 173–301.
[10] D.G. Evans, X. Duan, Chem. Commun. (2006) 485–496.
[11] L. Shi, D. Li, J. Wang, S. Li, D.G. Evans, X. Duan, Clays Clay Miner. 53 (2005) 294–300.
[12] Z. Wang, E. Han, W. Ke, Prog. Org. Coat. 53 (2005) 29–37.
[13] Y. Wang, D. Zhang, Mater. Res. Bull. 46 (2011) 1963–1968.
[14] A.I. Khan, L. Lei, A.J. Norquist, D. O'Hare, Chem. Commun. (2001) 2342–2343.
[15] G. Fan, F. Li, D.G. Evans, X. Duan, Chem. Soc. Rev. 43 (2014) 7040–7066.
[16] Y. Zhao, X. Jia, G.I.N. Waterhouse, L.-Z. Wu, C.-H. Tung, D. O'Hare, T. Zhang, Adv. Energy Mater. 6 (2015) 1501974.
[17] M. Dinari, M.M. Momeni, Y. Ghayeb, J. Mater. Sci.: Mater. Electron. 27 (2016) 9861–9869.
[18] Y. Song, J. Wang, Z. Li, D. Guan, T. Mann, Q. Liu, M. Zhang, L. Liu, Microporous Mesoporous Mater. 148 (2012) 159–165.
[19] Y. Zhao, B. Li, Q. Wang, W. Gao, C.J. Wang, M. Wei, D.G. Evans, X. Duan, D. O'Hare, Chem. Sci. 5 (2014) 951–958.
[20] Y. Dou, S. Xu, X. Liu, J. Han, H. Yan, M. Wei, D.G. Evans, X. Duan, Adv. Funct. Mater. 24 (2014) 514–521.
[21] C. Chen, M. Yang, Q. Wang, J.-C. Buffet, D. O'Hare, J. Mater. Chem. A 2 (2014) 15102–15110.
[22] Q. Wang, D. O'Hare, Chem. Commun. 49 (2013) 6301–6303.
[23] L. Hickey, J.T. Kloprogge, R.L. Frost, J. Mater. Sci. 35 (2000) 4347–4355.
[24] U. Costantino, F. Marmottini, M. Nocchetti, R. Vivani, Eur. J. Inorg. Chem. 1998 (1998) 1439–1446.
[25] N. Iyi, T. Matsumoto, Y. Kaneko, K. Kitamura, Chem. Lett. 33 (2004) 1122–1123.
[26] N. Iyi, K. Tamura, H. Yamada, J. Colloid Interface Sci. 340 (2009) 67–73.
[27] F.R. Costa, A. Leuteritz, U. Wagenknecht, D. Jehnichen, L. Häußler, G. Heinrich, Appl. Clay Sci. 38 (2008) 153–164.
[28] C. Yilmaz, U. Unal, H. Yagci Acar, J. Solid State Chem. 187 (2012) 295–299.
[29] M. Kayano, M. Ogawa, Clays Clay Miner. 54 (2006) 382–389.
[30] F. Kovanda, D. Koloušek, Z. Cílová, V. Hulínský, Appl. Clay Sci. 28 (2005) 101–109.
[31] A. Faour, V. Prévot, C. Taviot-Guého, J. Phys. Chem. Solids 71 (2010) 487–490.
[32] F.M. Labajos, V. Rives, M.A. Ulibarri, J. Mater. Sci. 27 (1992) 1546–1552.
[33] F. Kovanda, T. Rojka, P. Bezdička, K. Jirátová, L. Obalová, K. Pacultová, Z. Bastl, T. Grygar, J. Solid State Chem. 182 (2009) 27–36.
[34] Q. Wang, D. O'Hare, Chem. Rev. 112 (2012) 4124–4155.

[35] Q. Wang, X. Zhang, J. Zhu, Z. Guo, D. O'Hare, Chem. Commun. 48 (2012) 7450–7452.
[36] W. Qian, R. Hao, Y. Hou, Y. Tian, C. Shen, H. Gao, X. Liang, Nano Res. 2 (2009) 706–712.
[37] H. Chen, F. Zhang, S. Fu, X. Duan, Adv. Mater. 18 (2006) 3089–3093.
[38] Z.P. Xu, Y. Jin, S. Liu, Z.P. Hao, G.Q.M. Lu, J. Colloid Interface Sci. 326 (2008) 522–529.
[39] J.B. Han, J. Lu, M. Wei, Z.L. Wang, X. Duan, Chem. Commun. (2008) 5188.
[40] M. Ogawa, H. Kaiho, Langmuir 18 (2002) 4240–4242.
[41] C. Chen, A. Wangriya, J.-C. Buffet, D. O'Hare, Dalton Trans. 44 (2015) 16392–16398.
[42] W.L. Earl, D.L. Vanderhart, J. Magn. Reson. 48 (1982) 35–54.
[43] N. Gerds, V. Katiyar, C.B. Koch, J. Risbo, D. Plackett, H.C.B. Hansen, Appl. Clay Sci. 65-66 (2012) 143–151.
[44] S. Carlino, Solid State Ionics 98 (1997) 73–84.
[45] R. Celis, M.Á. Adelino, B. Gámiz, M.C. Hermosín, W.C. Koskinen, J. Cornejo, Appl. Clay Sci. 96 (2014) 81–90.
[46] L. Moyo, N. Nhlapo, W.W. Focke, J. Mater. Sci. 43 (2008) 6144–6158.
[47] H. Chen, F. Zhang, T. Chen, S. Xu, D.G. Evans, X. Duan, Chem. Eng. Sci. 64 (2009) 2957–2962.
[48] M. Nosonovsky, B. Bhushan, Curr. Opin. Colloid Interface Sci. 14 (2009) 270–280.
[49] N. Nhlapo, T. Motumi, E. Landman, S.M.C. Verryn, W.W. Focke, J. Mater. Sci. 43 (2007) 1033–1043.
[50] N.P. Funnell, Q. Wang, L. Connor, M.G. Tucker, D. O'Hare, A.L. Goodwin, Nanoscale 6 (2014) 8032–8036.
[51] E. Gardner, K.M. Huntoon, T.J. Pinnavaia, Adv. Mater. 13 (2001).
[52] G. Hu, D. O'Hare, J. Am. Chem. Soc. 127 (2005) 17808–17813.
[53] J. Zhang, X. Xie, C. Li, H. Wang, L. Wang, RSC Adv. 5 (2015) 29757–29765.
[54] W. Reichle, J. Catal. 101 (1986) 352–359.
[55] T. Isobe, T. Watanabe, J.B. d'Espinose de la Caillerie, A.P. Legrand, D. Massiot, J. Colloid Interface Sci. 261 (2003) 320–324.
[56] A. Abraham, R. Prins, J.A. van Bokhoven, E.R.H. van Eck, A.P.M. Kentgens, J. Phys. Chem. B 110 (2006) 6553–6560.